

LARGE AMPLITUDE OSCILLATORY SHEAR OF THE PRANDTL ELEMENT ANALYSED BY FOURIER TRANSFORM RHEOLOGY

MARTIN BOISLY*, MARKUS KÄSTNER, JÖRG BRUMMUND, VOLKER ULBRICHT

Institute of Solid Mechanics, Technische Universität Dresden, 01062 Dresden, Germany

*Corresponding author: martin.boisly@tu-dresden.de

Fax: x49.351.46337061

Received: 4.12.2013, Final version: 5.3.2014

ABSTRACT:

This work contributes to the theory of strain controlled large amplitude oscillatory shear (LAOS) as well as modelling the key properties of type III behavior of Hyun, the decreasing storage modulus and a loss modulus with considerable maximum. The latter two can be modelled with the help of the Prandtl element. Since it is a yield stress fluid, the use of LAOS is necessary to calculate the storage and loss modulus. Furthermore, a condition is presented which has to be met in order to avoid even harmonics. The storage and loss modulus as well as the higher harmonics of the Prandtl element are determined analytically in this work. They are given as mathematical functions which can be discussed conveniently. This allows the identification of characteristic points which are related to material parameters of the Prandtl element and enable a physically motivated material parameter identification. Beside this, it is observed that the yield strain do not coincide with the crossover $G'(\hat{\gamma}) = G''(\hat{\gamma})$ but with the increasing of the loss modulus and the decreasing of the storage modulus. Thanks to the analytical calculations, it is also obvious that the stress response of yield stress fluids does not necessarily include even harmonics. In this work the steady state stress response of the Prandtl element is also presented as Lissajous plots and Pipkin diagrams to visualise the rheological fingerprint.

KEY WORDS:

large amplitude oscillatory shear, Fourier Transform rheology, harmonic analysis, storage modulus, loss modulus, yield strain, Prandtl element, Lissajous plot, Pipkin diagram

1 INTRODUCTION

In recent years, strain controlled large amplitude oscillatory shear (LAOS) has been developed into a powerful tool to investigate non-linear material behavior. Therefore, a sinusoidal strain is imposed and the stress response is measured. The latter can be decomposed by a harmonic analysis, the Fourier Transform (FT) rheology [1–11], into the storage modulus G' , the loss modulus G'' as well as the higher harmonics a_k and b_k . These are material functions which tell about the material behavior and help drawing conclusions about model assumptions. Based on these, one can create a material model and is able to do further simulations. The storage and loss modulus can be also used for material classification. For example Hyun et al. [10] presented a classification depending on the LAOS behavior of $G'(\hat{\gamma})$ and $G''(\hat{\gamma})$ which consists of four types. Another way to present the characteristic of materials is the visualisation of their stress responses. Here it has become established to plot the Lissajous curves as well as the Pipkin

diagrams, the so called rheological fingerprint [12–14]. Furthermore, sinusoidal loading is an useful tool to investigate the rate-dependency $\dot{\gamma} \sim \hat{\gamma}\omega$ within a limited range of strain $-\hat{\gamma} \leq \gamma \leq \hat{\gamma}$ by varying the angular frequency ω [3, 10, 11, 15]. Thus, the critical strain γ_{cr} , which describes the limit of linearity to separate the range of small amplitude oscillatory shear (SAOS) from LAOS, can be determined within a high sensitivity investigation [8, 16]. After passing the limit of linearity the Fourier analysed stress response contains higher harmonics. Often the lack of physical interpretation of these higher harmonics is emphasised [17–20]. For improvement, new approaches have been suggested like (1) the Fourier Chebyshev analysis of Ewoldt [19] applying the stress decomposition of Cho [18], (2) the method of Klein [21] using sine, square, triangular and sawtooth waveforms as four fundamental basis functions, and (3) the sequence of physical processes technique of Rogers [15]. Further details as well as the state of the art are summarised elsewhere [11, 20, 22–24] making such a discussion redundant at this place.

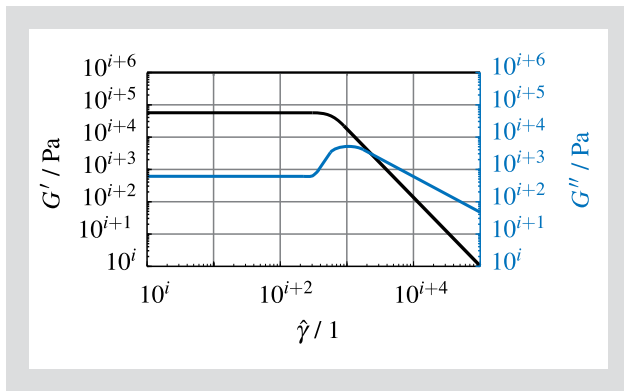


Figure 1: Qualitative plot of a decreasing storage modulus and a loss modulus with considerable maximum denoted as type III behaviour by Hyun et al. [10].

However, data information obtained by FT rheology are very useful for material modelling which is shown exemplarily for the Prandtl element in this work. Its key properties are the decreasing storage modulus and a loss modulus with considerable maximum according to Figure 1, which are typical for many materials like xanthan gum [9–11, 25], bioinspired slime [12], water based dispersions and emulsions [21], gastric mucin [26], magnetorheological fluids [27, 28], carbopol gel [29], colloidal glasses [30] as well as suspensions of soft colloids [17, 31]. In the sense of the classification of Hyun et al. [10] these features are denoted as type III behavior. Thus, this article is a theoretical work concerning generalities of large amplitude oscillatory shear and its application to the Prandtl element to be able to predict the LAOS behavior of more complex material models which partially can consist of a Prandtl element. Thereby, some theoretical findings are observed which result a priori from the constitutive equations. They show the need to be careful about conclusions that are drawn a posteriori about material systems by experimental analysis methods. This indeed is the quintessence of the discussion about the yield stress concept [32–34]: If a yield stress model is assumed to reproduce measurements, its yield point is given a priori so that one can postulate a posteriori the measurement point of yielding. The Prandtl element belongs to the class of yield stress fluids, as defined by Boisly [35]. According to the non-linear property of yield stress fluids, the range of small amplitude oscillatory shear is left. Hence, the use of large amplitude oscillatory shear is necessary. In Section 2 the storage and loss modulus as well as higher harmonics are defined by Equations 5 and 6, whereat even higher harmonics vanish if Equation 9 is fulfilled. This theory is applied to the Prandtl element in Section 3. First of all, its constitutive equations are briefly summarised in Section 3.1. Then, the storage and loss modulus and the higher harmonics as well as the Lissajous plots and the Pipkin diagrams are calculated in Section 3.2. The Lissajous curves as well as the storage and loss modulus show similarly a sharp transition from the preyield regime to the postyield because the constitutive equations of the

Prandtl element contain a yield function and a yield condition. The sharp transition is expressed by the sudden increase of $G''(\dot{\gamma})$ and the decrease of $G'(\dot{\gamma})$ of the Prandtl element after passing the critical strain according to Equation 24. In case of Lissajous curves, the sharp transition is given by sharp corners. Thus, independent from the fact that the storage and loss modulus are quantities which integrate the signal over the period according to Equations 5 and 6, they are able to detect the sharp transition if an amplitude sweep is considered.

A great benefit of this work arises from the fact that the calculations could be done analytically so that the LAOS response and the material functions are given explicitly in terms of mathematical functions. This is very useful in many steps of phenomenological material modelling. Generally, it is enough to calculate the LAOS behavior of a material model, either analytically or numerically, if its material parameters are fixed. This work also supports the circumstance where the material parameters are not given but still have to be determined. Here, the knowledge of analytically expressed material functions is productive which was also emphasised by Giacomini et al. [23]. They make the identification of material parameters as easy as possible [36]. With the help of analytically given material functions, characteristic points can be identified. Due to this, the influence of the material parameters on characteristic points of the storage and loss modulus as well as higher harmonics is given. Thus, a physically motivated parameter identification can be applied based on characteristic points. In principle, there is only one point that is relevant for the Prandtl element to identify its material parameters. However, to give the best possible analysis all characteristic points of the Prandtl element are presented. In particular, this is useful if the LAOS behavior of more complex material models which partially can consist of a Prandtl element has to be analysed. According to a curve sketching of these analytical functions, it is shown for the Prandtl element that the crossover between the storage and loss modulus does not coincide with the critical or yield strain as often assumed [17, 30, 31, 37–40]. Furthermore, it can be understood that the stress responses of yield stress fluids do not include even harmonics imperatively as it is sometimes considered [1, 21, 41–43]. Beside this, analytical material responses can also be used to check numerically implemented material models by the agreement between the prediction of the numerical implementation and the analytically given response. Thus, the aims of this work are

- the general definition of the storage and loss modulus and higher harmonics in case of LAOS,

- the presentation of a condition which has to be met in order to avoid even harmonics,
- to propose a rheological element, the Prandtl element, which is able to model the decreasing storage modulus and a loss modulus with considerable maximum of type III behavior of Hyun et al. [10],
- the fully analytical investigation of the Prandtl element with respect to strain controlled sinusoidal loading in the LAOS regime,
- the analytical description of the storage modulus, the loss modulus, higher harmonics, the Lissajous plots in Mode 1 and 2 as well as the Pipkin diagrams of the Prandtl element for LAOS which for example enable a verification of numerically implemented material models which include the Prandtl element,
- the identification of characteristic points of these material functions to improve the process of material modelling and to introduce a physically motivated material parameter identification.

2 STEADY STATE STRESS RESPONSE TO STRAIN CONTROLLED SINUSOIDAL LOADING

In this section strain controlled sinusoidal loading

$$\gamma(t) = \hat{\gamma} \sin(\omega t) \text{ with } : \hat{\gamma} > 0, \omega > 0 \quad (1)$$

and its general stress response are examined without referring to specific material models. The transient stress response of a rheological element according to this strain load is given by $\tau(t)$. In the following, it is assumed that it reaches the steady state stress

$$\tau_{\infty}(t) := \text{STEADYSTATE} \left\{ \tau(t) \Big|_{\gamma = \hat{\gamma} \sin(\omega t)} \right\} = \tau(t > t_o) \quad (2)$$

The operator $\text{STEADYSTATE}\{\}$ introduces t_o as parameter which defines the time henceforward the transient stress response is in steady state. Thus, it is a periodic function with the period of the strain load $T = 2\pi/\omega$ and satisfies $\tau_{\infty}(t) = \tau_{\infty}(t + T)$. Depending on $\hat{\gamma}$, two regions are distinguished, the small and large amplitude oscillatory shear.

2.1 SMALL AMPLITUDE OSCILLATORY SHEAR (SAOS)

In some cases the strain amplitudes are smaller than a critical strain γ_{cr} . In the range $0 \leq \hat{\gamma} \leq \gamma_{cr}$ the material behavior is characterised by a linear operator. The linear regime is observed for small amplitude oscillatory shear [11, 24, 44, 45]. Here, the steady state stress $\tau_{\infty}(t)$

of the transient stress response $\tau(t)$ related to strain controlled sinusoidal loading according to Equation 1 is given by

$$\tau_{\infty}(t) = \hat{\gamma} [G'(\omega) \sin(\omega t) + G''(\omega) \cos(\omega t)] \quad (3)$$

The storage modulus G' and the loss modulus G'' must not be functions of the strain amplitude [9, 11, 44] to fulfil the conditions of linearity.

2.2 LARGE AMPLITUDE OSCILLATORY SHEAR (LAOS)

For higher strain amplitudes with $\hat{\gamma} > \gamma_{cr}$, the large amplitude oscillatory shear [3, 11, 13, 24, 44, 46] is present so that the material behavior cannot be expressed by a linear operator. In this sense LAOS has to be seen as abbreviation for LAOStrain to differ it from LAOStress [13, 25, 47, 48]. Its steady state stress response generally can be expressed as a Fourier series [13, 28, 45, 49]

$$\tau_{\infty}(t) = \hat{\gamma} \sum_{k=1}^{\infty} [a_k(\omega, \hat{\gamma}) \sin(k\omega t) + b_k(\omega, \hat{\gamma}) \cos(k\omega t)] \quad (4)$$

including odd as well as even harmonics in general [13, 50, 51]. The Fourier coefficients

$$a_k(\omega, \hat{\gamma}) := \frac{2}{\hat{\gamma} T} \int_{t_o}^{t_o+T} \tau(t) \sin(k\omega t) dt \quad (5)$$

$$b_k(\omega, \hat{\gamma}) := \frac{2}{\hat{\gamma} T} \int_{t_o}^{t_o+T} \tau(t) \cos(k\omega t) dt \quad (6)$$

are generally functions of the angular frequency as well as the strain amplitude and are valid also for nonlinear material behavior. The storage and loss modulus result from

$$G'(\omega, \hat{\gamma}) := a_1(\omega, \hat{\gamma}) \quad (7)$$

$$G''(\omega, \hat{\gamma}) := b_1(\omega, \hat{\gamma}) \quad (8)$$

Since the steady state does not appear instantaneous for any material after the load is applied, the storage and loss modulus as well as the higher harmonics depend on the time of observation. That is why the parameter t_o defines the begin of integration so that the interval $t_o \leq t \leq t_o + T$ represents the steady state

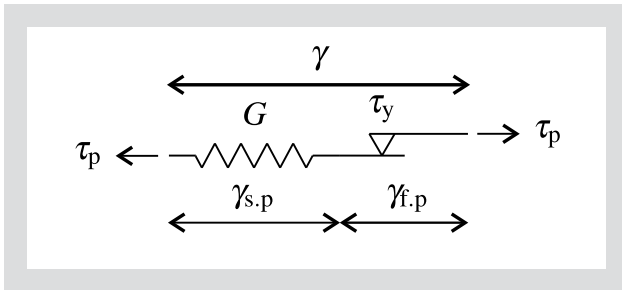


Figure 2: Rheological symbol of a Prandtl element.

stress response. If one furthermore restrict the steady state stress response to be a function with

$$\tau(t_o + \Delta t) = -\tau\left(t_o + \frac{T}{2} + \Delta t\right) \quad (9)$$

so that the first half of a period equals the negative of the second half of a period, the even harmonics vanish. Hence, the steady state stress is given only by the odd harmonics

$$\tau_\infty(t) = \hat{\gamma} \sum_{k, \text{odd}} [a_k(\omega, \hat{\gamma}) \sin(k\omega t) + b_k(\omega, \hat{\gamma}) \cos(k\omega t)] \quad (10)$$

with $k = 2n - 1$ for $n \in \mathbb{N}^+$. Since Equation 9 also can be true for yield stress fluids, their stress responses does not include even harmonics imperatively as it is sometimes considered [1, 21, 41–43]. This can be seen for example in case of the Prandtl element in Section 3.2. To decide how many higher harmonics have to be taken into account to simulate a non-linear behavior with a required accuracy, first of all the intensities

$$I_k(\omega, \hat{\gamma}) := \sqrt{a_k^2(\omega, \hat{\gamma}) + b_k^2(\omega, \hat{\gamma})} \quad (11)$$

are determined. It is derived if Equation 4 is transformed into the amplitude-phase description

$$\tau_\infty(t) = \hat{\gamma} \sum_{k=1}^{\infty} I_k \cos(k\omega t - \phi_k) \approx \hat{\gamma} \sum_{i=1}^m I_i \cos(i\omega t - \phi_i) \quad (12)$$

with

$$\phi_k := \arctan\left(\frac{a_k}{b_k}\right) \quad (13)$$

With the help of the higher harmonic contribution [7, 9] given by the normalised intensities I_k/I_1 , the parameter m of Equation 12 can be determined.

3 ANALYTICAL CALCULATIONS OF THE LARGE AMPLITUDE OSCILLATORY SHEAR RESPONSE OF THE PRANDTL ELEMENT

3.1 ONE-DIMENSIONAL CONSTITUTIVE EQUATIONS OF THE PRANDTL ELEMENT

The Prandtl element represents a yield stress fluid, as defined by Boisly [35], because it has a non-zero equilibrium relation according to relaxation and a well defined flow function. Since it is a rate-independent material model, it considers solely plastic flow. Hence, viscous properties may not exist from the flow function which can be exclusively satisfied if the viscosity is defined as differential viscosity. This is shown in detail in Boisly [35]. The Prandtl element has an elastic range and plastic properties without hardening effects as illustrated in Figure 2. The parameter G is the elastic modulus of the Hookean spring and τ_y is the yield stress of the friction element [35]. With respect to the kinematic and kinetic conditions of a series connection, it follows

$$\tau_p = G\gamma_{s,p} \quad (14a)$$

$$\tau_p = \tau_y \widetilde{\text{sign}}(\dot{\gamma}_{f,p}) \quad (14b)$$

$$\gamma = \gamma_{s,p} + \gamma_{f,p} \quad (14c)$$

with

$$\widetilde{\text{sign}}(\dot{\gamma}_{f,p}) = \begin{cases} -1 & : \dot{\gamma}_{f,p} < 0 \\ \xi & : \dot{\gamma}_{f,p} = 0 \text{ with } -1 < \xi < 1 \\ 1 & : \dot{\gamma}_{f,p} > 0 \end{cases} \quad (15)$$

The definition $\widetilde{\text{sign}}(0) = \xi$ is chosen in contrast to the ordinary definition $\text{sign}(0) = 0$ of Equation 20 to take $-\tau_y < \tau_p < \tau_y$ into account if $\dot{\gamma}_{f,p} = 0$. In this sense the variable ξ is determined by the equilibrium so that also the material behavior in case of vanishing plastic flow can be expressed. Thus, ξ lies in the interval $-1 < \xi < 1$. The loading and unloading behavior is given in the most convenient formulation analog to the friction element by the yield function $F(\tau_p) = |\tau_p| - \tau_y$, the Karush-Kuhn-Tucker conditions and the consistency condition [35]. Since the strain of the Prandtl element is a sum of $\gamma_{s,p}$ and $\gamma_{f,p}$, each one cannot be determined directly for a given strain history $\gamma(t)$. This implicates the choice of an internal variable of a strain type. Here, the strain of the friction element is chosen. Its evolution results from the associated flow rule

$$\dot{\gamma}_{f,p} = \zeta \frac{\partial F}{\partial \tau_p} \quad (16)$$

To define the proportionality factor ζ , $\dot{F} = 0$ is evaluated. One obtains the evolution equation

$$\dot{\gamma}_{f,p} = \dot{\gamma} \text{ if } (F = 0) \wedge (\dot{F} = 0) \quad (17)$$

With the help of Equations 14b and 17 the general condition

$$\widehat{\text{sign}}(\tau_p) = \widehat{\text{sign}}(\dot{\gamma}_{f,p}) = \widehat{\text{sign}}(\dot{\gamma}) \text{ if } (F = 0) \wedge (\dot{F} = 0) \quad (18)$$

is found. The proportionality factor yields

$$\zeta = |\dot{\gamma}| \text{ if } (F = 0) \wedge (\dot{F} = 0) \quad (19)$$

according to Equations 16, 17, 18, and $\partial F / \partial \tau_p = \text{sign}(\tau_p)$ with the ordinary signum function

$$\text{sign}(x) = \begin{cases} -1 & : x < 0 \\ 0 & : x = 0 \\ 1 & : x > 0 \end{cases} \quad (20)$$

Thus, the evolution equation of the internal variable $\gamma_{f,p}$. Equation 16 also can be expressed by

$$\dot{\gamma}_{f,p} = |\dot{\gamma}| \text{sign}(\tau_p) \text{ if } (F = 0) \wedge (\dot{F} = 0) \quad (21)$$

but cannot be determined without knowing the absolute value of the strain rate at which $\tau_p = \tau_y$ or $\tau_p = -\tau_y$ is applied. The preyield and postyield are defined analog to the friction element as it is done in Boily [35].

3.2 LARGE AMPLITUDE OSCILLATORY SHEAR OF THE PRANDTL ELEMENT

In the following, the material behavior of a Prandtl element is investigated related to a sinusoidal strain loading $\gamma = \hat{\gamma} \sin(\omega t)$ under the initial conditions

$$\tau_p(t=0) = 0 \quad (22)$$

i	t_i	$\gamma _{t_i}$	$\gamma_{f,p} _{t_i}$
0	0	0	0
1	$\left[\arcsin\left(\frac{\tau_y}{G\hat{\gamma}}\right) \right] \frac{1}{\omega}$	$\frac{\tau_y}{G}$	0
2	$\frac{\pi}{2\omega}$	$\hat{\gamma}$	$\hat{\gamma} - \frac{\tau_y}{G}$
3	$\left[\pi - \arcsin\left(1 - \frac{2\tau_y}{G\hat{\gamma}}\right) \right] \frac{1}{\omega}$	$\hat{\gamma} - \frac{2\tau_y}{G}$	$\hat{\gamma} - \frac{\tau_y}{G}$
4	$\frac{3\pi}{2\omega}$	$-\hat{\gamma}$	$-\left(\hat{\gamma} - \frac{\tau_y}{G}\right)$
5	$\left[2\pi + \arcsin\left(\frac{2\tau_y}{G\hat{\gamma}} - 1\right) \right] \frac{1}{\omega}$	$-\left(\hat{\gamma} - \frac{2\tau_y}{G}\right)$	$-\left(\hat{\gamma} - \frac{\tau_y}{G}\right)$
6	$\frac{5\pi}{2\omega}$	$\hat{\gamma}$	$\hat{\gamma} - \frac{\tau_y}{G}$

Table 1: t_i , $\gamma|_{t_i}$, and $\gamma_{f,p}|_{t_i}$ for sinusoidal strain loading $\gamma = \hat{\gamma} \sin(\omega t)$ with $i = 0 \dots 6$.

$$\gamma_{f,p}(t=0) = 0 \quad (23)$$

The latter restriction, Equation 23, is necessary because in general every non-zero strain of the friction element [35] can satisfy Equation 22 which would shift Equation 24. The Prandtl element acts in the preyield and fulfils the condition of SAOS if it is harmonically loaded by strain amplitudes less or equal than the critical strain

$$\gamma_{cr} = \frac{\tau_y}{G} \quad (24)$$

In this case, it behaves linear like a Hookean spring. Hence the storage modulus equals G and the loss modulus is zero. In the following, the LAOS behavior of the Prandtl element is investigated for $\hat{\gamma} > \gamma_{cr}$. Since the stress response is not instantaneously in steady state, $\tau_{p,\infty} \neq \tau_p|_{\gamma = \hat{\gamma} \sin(\omega t)}$, it is calculated as long as the first period being representative for steady state. If the values of the internal variable $\gamma_{f,p}$ at the beginning and the end of a period are the same, the period represents steady state. The LAOS stress response is given by

$$\tau_p(t)|_{\gamma = \hat{\gamma} \sin(\omega t)} = \begin{cases} G\gamma & : 0 \leq t \leq t_1 \\ \tau_y & : t_1 \leq t \leq t_2 \\ G(\gamma - \gamma_{f,p}|_{t_2}) & : t_2 \leq t \leq t_3 \\ -\tau_y & : t_3 \leq t \leq t_4 \\ G(\gamma - \gamma_{f,p}|_{t_4}) & : t_4 \leq t \leq t_5 \\ \tau_y & : t_5 \leq t \leq t_6 \end{cases} \quad (25)$$

and plotted in Figure 3a. The evolution of the internal variable is calculated by $\gamma_{f,p} = \gamma - \tau_p/G$ and is plotted in Figure 3b. The values of the parameters which are used in Equation 25 are defined in Table 1 with respect to the domain of definition of the arc sine function. Since the values of the internal variable at the times t_2 and t_6 are the same $\gamma_{f,p}|_{t_2} = \gamma_{f,p}|_{t_6}$, the first period which represents

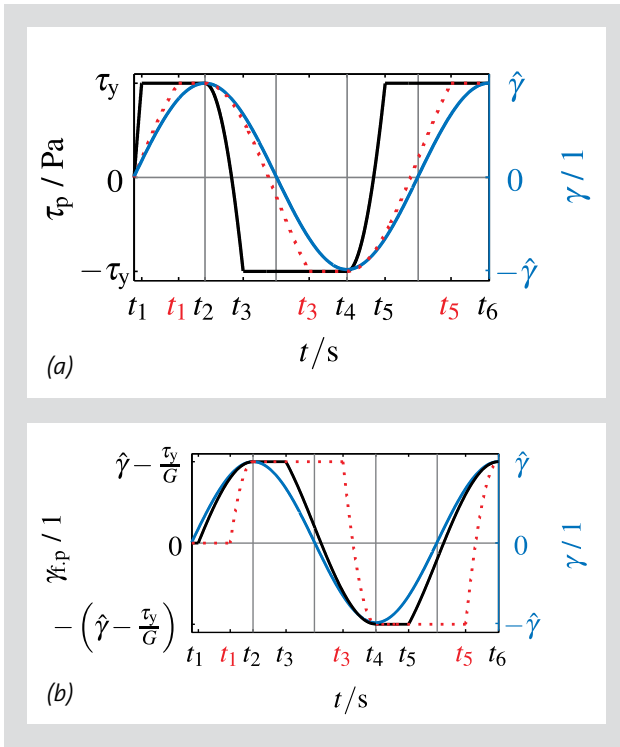


Figure 3: (a) Stress response and (b) response of the internal variable $\gamma_{f,p}$ related to sinusoidal loading with $\omega = 2\pi / s$ and $\hat{\gamma} = 1.5$ (Mode 1 — for $G/\tau_y = 4$, Mode 2 for $G/\tau_y = 0.8$).

steady state lies in between $t_2 \leq t \leq t_6$. Depending on t_3 , the postyield of the PRANDTL element can be classified into two modes which can be seen in Figures 3, 7, and 8. In case of Mode 1 the postyield is present for more than the half of a period being representative for steady state. Thus, Mode 1 occurs for $\pi/(2\omega) < t_3 \leq \pi/\omega$ which equals

$$\text{MODE1: } \frac{\tau_y}{G\hat{\gamma}} \leq \frac{1}{2} \quad (26)$$

relating to the analytical expression for t_3 . The consequences are a large hysteresis of the first Lissajous plot (Figure 7a) and overlapping parts of the second Lissajous plot (Figure 7b). In Mode 2 the postyield appears less than the half of a steady state period so that the hysteresis of the first Lissajous plot is smaller than the one of Mode 1. Furthermore, no overlapping occurs in the second Lissajous plot. Mode 2 is given by $\pi/\omega < t_3 < 3\pi/(2\omega)$ which is identical to $1/2 < \tau_y/(G\hat{\gamma}) < 1$. Its upper limit

$$\text{MODE2 (upper limit): } \frac{\tau_y}{G\hat{\gamma}} < 1 \quad (27)$$

ensures being in the postyield. Its lower limit

$$\text{MODE2 (lower limit): } \frac{\tau_y}{G\hat{\gamma}} > \frac{1}{2} \quad (28)$$

stands for the transition from Mode 2 to Mode 1. As it can be seen in Figures 3a and 3b, the transition occurs for $t_3 = \pi/\omega$ which is accompanied with $\tau_y/(G\hat{\gamma}) = 1/2$. This is found according to the analytical expression $t_3 = [\pi - \arcsin(1 - 2\tau_y/(G\hat{\gamma}))]/\omega$ of Table 1. Finally, Equations 26, 27, and 28 can be transformed into

$$\text{MODE1: } \frac{2\tau_y}{G} \leq \hat{\gamma} \quad (29)$$

$$\text{MODE2: } \frac{\tau_y}{G} < \hat{\gamma} < \frac{2\tau_y}{G} \quad (30)$$

To determine the storage and loss modulus, Equations 5 to 8 have to be considered because the Prandtl element is a non-linear model. Therefore, $t_o = t_2$ because t_2 defines the beginning of the first period of steady state. Thus, the storage modulus in case of $\hat{\gamma} > \gamma_{cr}$ is given by $G'_p(\omega, \hat{\gamma}) = 2/(\hat{\gamma}T) \int_{t_2}^{t_2+T} \tau_p(t) \sin(\omega t) dt$. Considering $\tau_p(t_2 + \Delta t) = -\tau_p(t_2 + T/2 + \Delta t)$, which is also valid for the sine and cosine function, as well as $t_2 + T/2 = t_4$, the storage modulus in case of $\hat{\gamma} > \gamma_{cr}$ is calculated by $G'_p(\omega, \hat{\gamma}) = 4/(\hat{\gamma}T) \int_{t_2}^{t_4} \tau_p(t) \sin(\omega t) dt$. Thus, the storage modulus of the Prandtl element can be summarised into

$$\hat{\gamma} \leq \gamma_{cr}: G'_p(\hat{\gamma}) = G \quad (31)$$

$$\hat{\gamma} > \gamma_{cr}: G'_p(\hat{\gamma}) = G \left\{ \frac{1}{2} + \frac{1}{2\pi} \sin \left[2 \arcsin \left(1 - \frac{2\tau_y}{G\hat{\gamma}} \right) \right] - \frac{1}{\pi} \arcsin \left[1 - \frac{2\tau_y}{G\hat{\gamma}} \right] + \frac{4}{\pi} \sqrt{\frac{\tau_y}{G\hat{\gamma}}} \left(\frac{2\tau_y}{G\hat{\gamma}} - 1 \right) \sqrt{1 - \frac{\tau_y}{G\hat{\gamma}}} \right\} \quad (32)$$

The plausibility of Equation 32 is proved by the condition of continuity

$$G'_p \left(\hat{\gamma} = \frac{\tau_y}{G} \right) = G \quad (33)$$

between the cases $\hat{\gamma} \leq \gamma_{cr}$ and $\hat{\gamma} > \gamma_{cr}$ which denotes a characteristic point. Beside this, it yields

$$G'_p \left(\hat{\gamma} = \frac{2\tau_y}{G} \right) = \frac{G}{2} \quad (34)$$

Furthermore, it applies

$$\lim_{\hat{\gamma} \rightarrow \infty} G'_p = 0 \quad (35)$$

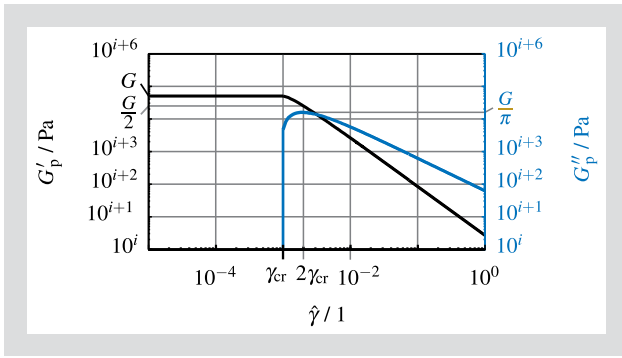


Figure 4: Qualitative plot of the storage and loss modulus depending on the strain amplitude of the Prandtl element for $\gamma_{cr} = \tau_y/G$, $G = 5 \cdot 10^4$ Pa, and $\tau_y = 50$ Pa.

The derivation of the loss modulus is analog to the discussion of the storage modulus. It is given by $G_p''(\omega, \hat{\gamma}) = 4/(\hat{\gamma}T) \int_{t_2}^{t_4} \tau_p(t) \cos(\omega t) dt$ and yields

$$\hat{\gamma} \leq \gamma_{cr} : G_p''(\hat{\gamma}) = 0 \quad (36)$$

$$\hat{\gamma} > \gamma_{cr} : G_p''(\hat{\gamma}) = \frac{4\tau_y}{\hat{\gamma}\pi} \left(1 - \frac{\tau_y}{G\hat{\gamma}} \right) \quad (37)$$

With the help of the condition of continuity

$$G_p''\left(\hat{\gamma} = \frac{\tau_y}{G}\right) = 0 \quad (38)$$

between the cases $\hat{\gamma} \leq \gamma_{cr}$ and $\hat{\gamma} > \gamma_{cr}$ the plausibility of Equation 37 is proven. The maximum of the loss modulus is given by

$$\text{MAX}\{G_p''(\hat{\gamma})\} = G_p''\left(\hat{\gamma} = \frac{2\tau_y}{G}\right) = \frac{G}{\pi} \quad (39)$$

and marks another characteristic point of the Prandtl element. Furthermore,

$$\lim_{\hat{\gamma} \rightarrow \infty} G_p'' = 0 \quad (40)$$

The plot of $G_p'(\hat{\gamma})$ and $G_p''(\hat{\gamma})$ is given in Figure 4. It is often assumed, that the crossover $G'(\hat{\gamma}) = G''(\hat{\gamma})$ matches with the critical or yield strain [17, 30, 31, 37–40]. However, this does not hold for the Prandtl element. Here, the critical strain coincides with the increase of the loss modulus and the decrease of the storage modulus. Since the storage and loss modulus are independent of the angular frequency, the plots $G_p'(\omega)$ and $G_p''(\omega)$ are constants and not shown here. The calculation of the odd coefficients $a_{p,k,odd}$ with $k \geq 3$ is analog to that of the storage modulus $a_{p,k}(\omega, \hat{\gamma}) = 4/(\hat{\gamma}T) \int_{t_2}^{t_4} \tau_p(t) \sin(k\omega t) dt$ and can be summarised into

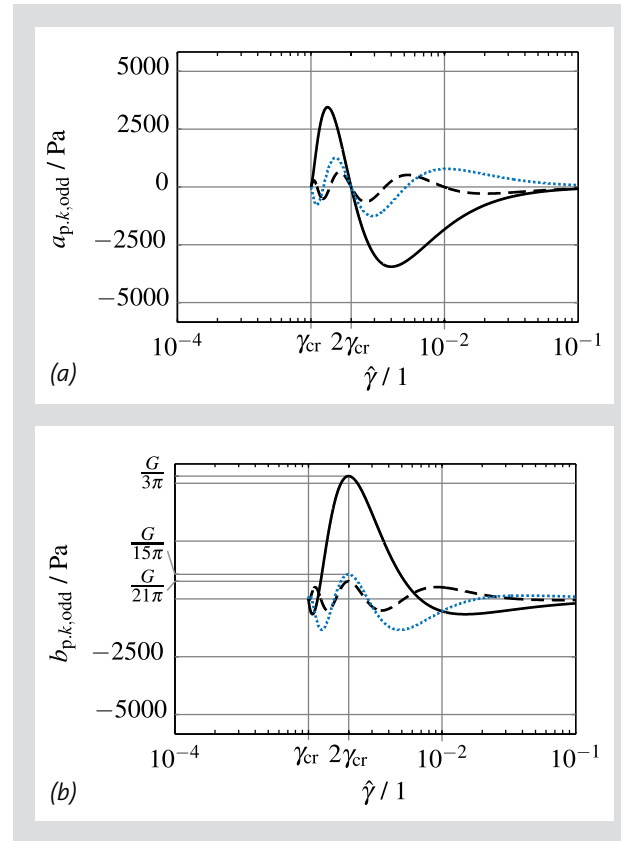


Figure 5: Plots of higher harmonics of the Prandtl element depending on the strain amplitude: (a) $a_{p,k,odd}(\hat{\gamma})$ and (b) $b_{p,k,odd}(\hat{\gamma})$ for $G = 5 \cdot 10^4$ Pa and $\tau_y = 50$ Pa with $k = 3$ —, $k = 5$ ·····, and $k = 7$ - - -.

$$\hat{\gamma} \leq \gamma_{cr} : a_{p,k,odd}(\hat{\gamma}) = 0 \quad (41)$$

$$\hat{\gamma} > \gamma_{cr} : a_{p,k,odd}(\hat{\gamma}) = \frac{G}{\pi} \left[\frac{\sin\left[(k+1)\arcsin\left(1 - \frac{2\tau_y}{G\hat{\gamma}}\right)\right]}{k+1} - \frac{\sin\left[(k-1)\arcsin\left(1 - \frac{2\tau_y}{G\hat{\gamma}}\right)\right]}{k-1} \right] + \frac{2\left(\frac{2\tau_y}{G\hat{\gamma}} - 1\right)\cos\left[k\arcsin\left(1 - \frac{2\tau_y}{G\hat{\gamma}}\right)\right]}{k} \quad (42)$$

Also the plausibility of Equation 42 can be proved by the condition of continuity

$$a_{p,k,odd}\left(\hat{\gamma} = \frac{\tau_y}{G}\right) = 0 \quad k = 2n+1, n \in \mathbb{N}^+ \quad (43)$$

In the limit case the odd higher harmonics tend to zero

$$\lim_{\hat{\gamma} \rightarrow \infty} a_{p,k,odd}(\hat{\gamma}) = 0 \quad k = 2n+1, n \in \mathbb{N}^+ \quad (44)$$

A further characteristic point is given by the root

$$a_{p,k,odd}\left(\hat{\gamma} = \frac{2\tau_y}{G}\right) = 0 \quad k = 2n+1, n \in \mathbb{N}^+ \quad (45)$$

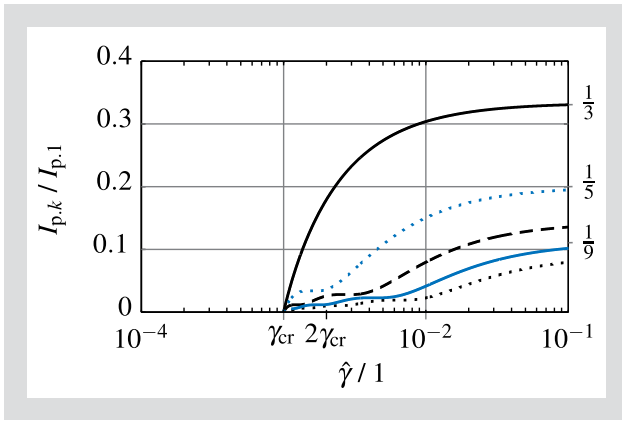


Figure 6: Plot of the normalised odd intensities of the Prandtl element depending on the strain amplitude for $G = 5 \cdot 10^4$ Pa and $\tau_y = 50$ Pa with $k = 3$ —, $k = 5$ ·····, $k = 7$ - - -, $k = 9$ — — —, and $k = 11$ ·····.

The dependency on the strain amplitude of $a_{p,k,odd}$ with $k = 3, 5, 7$ is plotted in Figure 5a. The odd coefficients $b_{p,k,odd}$ with $k \geq 3$ are given by

$$\hat{\gamma} \leq \gamma_{cr} : b_{p,k,odd}(\hat{\gamma}) = 0 \quad (46)$$

$$\hat{\gamma} > \gamma_{cr} : b_{p,k,odd}(\hat{\gamma}) = \frac{G}{\pi} \left[\frac{\cos\left[(k-1)\arcsin\left(1 - \frac{2\tau_y}{G\hat{\gamma}}\right)\right]}{k-1} - \frac{\cos\left[(k+1)\arcsin\left(1 - \frac{2\tau_y}{G\hat{\gamma}}\right)\right]}{k+1} \right] + \frac{2}{(k+1)(k-1)k} \left(-1\right)^{\frac{k+1}{2}} + \frac{2}{k} \left(\frac{2\tau_y}{G\hat{\gamma}} - 1\right) \sin\left[k \arcsin\left(1 - \frac{2\tau_y}{G\hat{\gamma}}\right)\right] \quad (47)$$

Analog to $a_{p,k,odd}$ the check of plausibility can be done by

$$b_{p,k,odd}\left(\hat{\gamma} = \frac{\tau_y}{G}\right) = 0 \quad k = 2n+1, n \in \mathbb{N}^+ \quad (48)$$

and in the limit case it yields

$$\lim_{\hat{\gamma} \rightarrow \infty} b_{p,k,odd}(\hat{\gamma}) = 0 \quad k = 2n+1, n \in \mathbb{N}^+ \quad (49)$$

Each maximum of an odd term with $k \geq 3$

$$\text{MAX}\{b_{p,k,odd}\} = b_{p,k,odd}\left(\hat{\gamma} = \frac{2\tau_y}{G}\right) = \frac{2G\left(k + (-1)^{\frac{k+1}{2}}\right)}{\pi(k+1)(k-1)k} \quad k = 2n+1, n \in \mathbb{N}^+ \quad (50)$$

defines the last characteristic point. In summary, three characteristic points were identified by the storage and loss modulus so that the elastic modulus G and the yield stress τ_y can be determined for example from the critical strain (Equation 24), the preyield-plateau of the storage modulus (Equation 33) or the maximum of the loss modulus (Equation 39). Characteristic points were also found in higher harmonics. Thus the root of $a_{p,k,odd}$ (Equation 45) and each maximum $\text{MAX}\{b_{p,k,odd}\}$ (Equation 50) can be used in addition to calculate G and τ_y . In

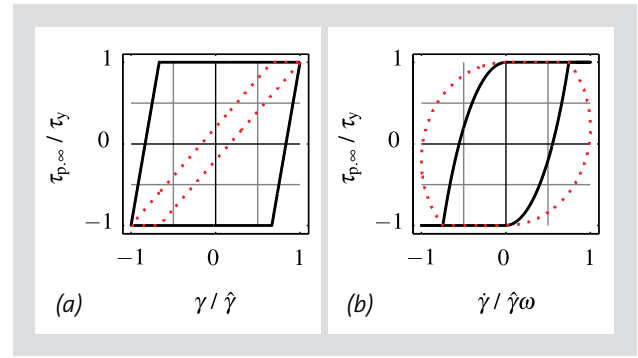


Figure 7: (a) First Lissajous and (b) second Lissajous plot of the Prandtl element related to sinusoidal loading with $\omega = 2\pi$ 1/s and $\hat{\gamma} = 1.5$ (Mode 1 — for $G/\tau_y = 4$, Mode 2 ····· for $G/\tau_y = 0.8$).

principle, not all of these points are relevant for the Prandtl element to identify its material parameters. However, to determine material parameters of soft matter whose LAOS behavior can partially modelled by a Prandtl element the knowledge of more characteristic points is useful. The graphs of the dependence of $b_{p,k,odd}$ on the strain amplitude is given in Figure 5b for $k = 3, 5, 7$. Since the SAOS, $\hat{\gamma} \leq \gamma_{cr}$, is accompanied with linear material behavior, both $a_{p,k}$ as well as $b_{p,k}$ with $k \geq 3$ equal zero. Furthermore, also the higher Fourier coefficients and normalised odd intensities are independent on the angular frequency, the graphs of $a_{p,k}(\omega)$, $b_{p,k}(\omega)$, and $I_{p,k}(\omega)/I_{p,1}(\omega)$ are constants and not plotted here. The normalised odd intensities $I_{p,k}(\hat{\gamma})/I_{p,1}(\hat{\gamma})$ are given in Figure 6 for $k = 3, 5, 7, 9, 11$. It can be seen that the normalised odd intensities, and thus also higher harmonics, become more dominant by increasing the strain amplitude. For the special choice of material parameters, $G = 5 \cdot 10^4$ Pa and $\tau_y = 50$ Pa, they tend until $\hat{\gamma} = 10^{-1}$ to the corresponding values of the friction element $I_{p,k}/I_{p,1} \approx I_{f,k}/I_{f,1} = 1/k$. Beside higher harmonics as well as the storage and loss modulus, the ordinary or normalised Lissajous plots [24, 25, 45, 52, 53] are common graphs to visualise the rheological fingerprint [12–14] of materials related to sinusoidal loading. The normalised Lissajous plots represent the normalised steady state stress $\tau_{\infty}(t)/\text{MAX}\{\tau_{\infty}(t)\}$ versus the normalised strain $\gamma(t)/\text{MAX}\{\gamma(t)\}$ and the normalised steady state stress versus the normalised strain rate $\dot{\gamma}(t)/\text{MAX}\{\dot{\gamma}(t)\}$ [54]. Here $\text{MAX}\{\{\}\}$ is an operator which determines the maximum of $\{\}$. The normalised Lissajous plots of Mode 1 and 2 are shown in Figure 7. In the first and second Lissajous plot (Figure 7a and 7b), a hysteresis occurs due to the plastic properties independent from the mode at which the Prandtl element works. Since in Mode 1 the ratio $G/(\tau_y\hat{\gamma})$ is smaller than in Mode 2, the hysteresis of the first Lissajous plot in Mode 1 is larger than in Mode 2. Since the normalised Lissajous plots of Mode 1 and 2 differ significantly from each other, it becomes clear that a rheological element does not have to have only one characteristic first and second Lissajous plot. Thus, all of the rheological properties get obvious only by the overview of first and second Lissajous plots represented by the first and second Pipkin diagram. The latter are plots about the full spec-

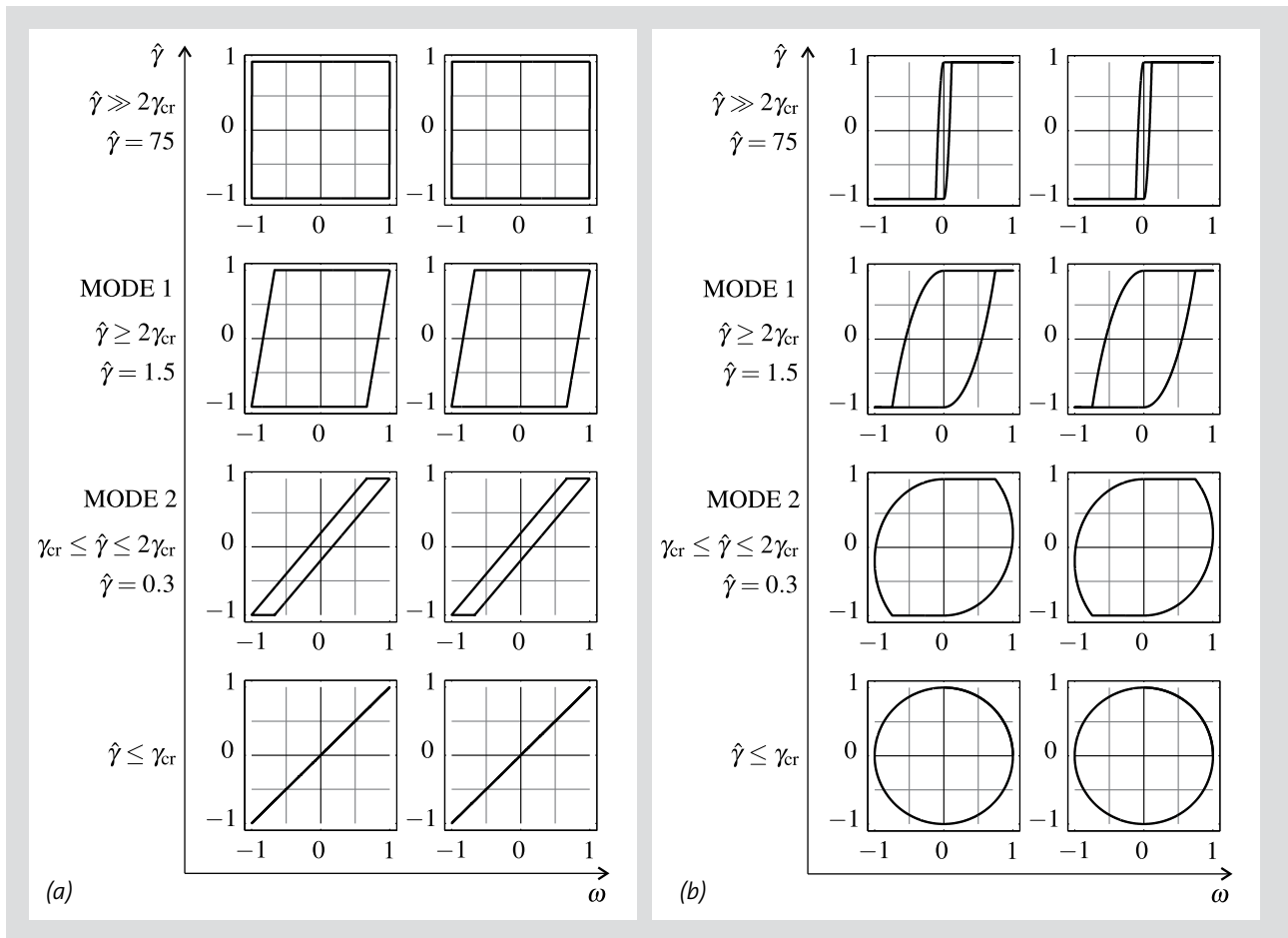


Figure 8: (a) First Pipkin diagram $\tau_{p,\infty}/\tau_y$ versus $\gamma/\hat{\gamma}$ and (b) second Pipkin diagram $\tau_{p,\infty}/\tau_y$ versus $\dot{\gamma}/(\hat{\gamma}\omega)$ of the Prandtl element with $G/\tau_y = 1/\gamma_{cr} = 4$.

trum of Lissajous plots of a material model [7]. Here the notion of Ewoldt [13, 19] is chosen which defines a Pipkin diagram as $\hat{\gamma} - \omega$ plot. The overview of the first and second Lissajous plots are shown in the first (Figure 8a) and second Pipkin diagram (Figure 8b). They can be used for example to identify rate-independent material behavior. The simplest rate-independent material is the elastic one. Here the Pipkin diagram of the first Lissajous plot is an open line. In case of the Prandtl element, this occurs for $\hat{\gamma} \leq \tau_y/G$ because it behaves in the preyield like a Hookean spring. The other rate-independent class of material behavior defined by Haupt [55] is plasticity. In this case the first Lissajous plot does not need to be an open line. Its shape depends on the strain amplitude but is independent of the angular frequency. This can be seen exemplarily for the Prandtl element when $\hat{\gamma} > \gamma_{cr}$ because it behaves plastic in the postyield. For $\hat{\gamma} \gg 2\gamma_{cr}$ the Prandtl element behaves like the friction element [35].

4 SUMMARY AND CONCLUSION

For yield stress fluids, as defined by Boisly [35], typical steady state LAOS behavior shows a decreasing storage modulus and a loss modulus with considerable maximum which are key properties of type III behavior of Hyun et al. [10]. They were modelled by the Prandtl ele-

ment in this work. Large amplitude oscillatory shear is present if material models begin to behave non-linear. In this sense ‘large’ means that the strain (or stress) amplitude are large enough to enforce a material specimen to behave non-linear. In Section 2 generalities of LAOS were briefly summarised and a condition was presented by Equation 9, which indicates the absence of even harmonics. The theory of LAOS was applied in Section 3 to the Prandtl element. Its constitutive equations were given in Section 3.1 so that the transient stress response could be calculated at the beginning of Section 3.2. Subsequently, the storage and loss modulus as well as the higher harmonics were determined. All of these calculations were done analytically which enable the:

- convenient use of the explicitly given mathematical function,
- determination of characteristic points and its relation to material parameters,
- physically motivated material parameter identification using characteristic points,
- verification of numerically implemented material models which include the Prandtl element.

In future works also the investigation of the medium amplitude oscillatory shear (MAOS) [11, 56, 57] is possible. General practical views can be theoretically compared with the MAOS of the Prandtl element. For the

Prandtl element three characteristic points were identified by the storage and loss modulus so that the elastic modulus G and the yield stress τ_y can be determined for example from the yield point: the critical strain (Equation 24) and the preyield-plateau of the storage modulus (Equation 33). The parameters also can be identified by the maximum point of the loss modulus according to Equation 39. Characteristic points were also found in higher harmonics. Thus the root of $a_{p,k,odd}$ (Equation 45) and each maximum $\text{MAX}\{b_{p,k,odd}\}$ (Equation 50) can be used in addition to calculate G and τ_y . In principle, there is only one point that is relevant for the Prandtl element to identify its material parameters. However, to determine material parameters of soft matter whose LAOS behavior can partially modelled by a Prandtl element the knowledge of more characteristic points is useful. Furthermore, it was observed that the critical strain does not have to coincide with the crossover $G'(\dot{\gamma}) = G''(\dot{\gamma})$ in any case. In case of the Prandtl element the beginning of the postyield results a priori by the constitutive equations. It happens at the critical strain which occurs at the increasing of the loss modulus and the decreasing of the storage modulus. This shows the need to be careful about conclusions that are drawn a posteriori about material systems by experimental analysis methods. Beside this, it was proved analytically that the LAOS stress response of yield stress fluids does not include even harmonics imperatively as it is sometimes considered. Even harmonics vanish in case of the Prandtl element because its stress response fulfil Equation 9. Another presentation of the LAOS behavior of the Prandtl element, its rheological fingerprint, was given by the Lissajous plots and the Pipkin diagrams. They were shown at the end of Section 3.2. Depending on $\tau_y/(G\dot{\gamma})$, the Prandtl element behave either in Mode 1 or Mode 2. Since they differ significantly from each other, it became clear that a rheological element does not necessarily generate only one characteristic first and second Lissajous plot. In general, it may has several typical Lissajous plots. Both modes have in common that the preyield and postyield parts are separated by sharp corners similarly to the storage and loss modulus. Latter also show a sharp transition from the preyield regime to the postyield at the critical strain because the constitutive equations of the Prandtl element contain a yield function and a yield condition. The sharp transition is expressed by the sudden increase of $G''(\dot{\gamma})$ and the decrease of $G'(\dot{\gamma})$. Thus, independent from the fact that the storage and loss modulus are quantities which integrate the signal over the period according to Equations 5 and 6, they are able to detect the yielding if an amplitude sweep is considered.

ACKNOWLEDGEMENTS

This project (ECEMP-B4; Nr.: 10011530) is funded by the European Union and the Free State of Saxony.

REFERENCES

- [1] Harris J, Bogie K: The experimental analysis of non-linear waves in mechanical systems, *Rheol. Acta* 6 (1967) 3–5.
- [2] Krieger IM, Niu TF: A rheometer for oscillatory studies of nonlinear fluids, *Rheol. Acta* 12 (1973) 567–571.
- [3] Giacomini AJ, Dealy JM: *Techniques in rheological measurements*, Chapman and Hall, London (1993).
- [4] Reimers KJ, Dealy JM: Sliding plate rheometer studies of concentrated polystyrene solutions: Large amplitude oscillatory shear of a very high molecular weight polymer in diethyl phthalate, *J. Rheol.* 40 (1996) 167–186.
- [5] Wilhelm M, Maring D, Spiess HW: Fourier-transform rheology, *Rheol Acta* 37 (1998) 399–405.
- [6] Wilhelm M, Reinheimer P, Ortseifer M: High sensitivity fourier-transformrheology, *Rheol. Acta* 38 (1999) 349–356.
- [7] Neidhöfer T, Wilhelm M, Spiess HW: Fourier-transform-rheology on linear polystyrene melts, *Appl. Rheol.* 11 (2001) 126–133.
- [8] Wilhelm M: Fourier-transform rheology, *Macromol. Mater. Eng.* 287 (2002) 83–105.
- [9] Franck A: A new generation of separate motor and transducer rheometers, *Appl. Rheol.* 18 (2008) 44–47.
- [10] Hyun K, Kim SH, Ahn KH, Lee SJ: Large amplitude oscillatory shear as a way to classify the complex fluids, *J. Non-Newton Fluid Mech.* 107 (2002) 51–65.
- [11] Hyun K, Wilhelm M, Klein CO, Cho KS, Nam JG, Ahn KH, Lee SJ, Ewoldt RH, McKinley GH: A review of nonlinear oscillatory shear tests: Analysis and application of large amplitude oscillatory shear (LAOS), *Prog. Polym. Sci.* 36 (2011) 1697–1753.
- [12] Ewoldt RH, Clasen C, Hosoi AE, McKinley GH: Rheological fingerprinting of gastropod pedal mucus and synthetic complex fluids for biomimicking adhesive locomotion, *Soft Matter* 3 (2007) 634–643.
- [13] Ewoldt RH: Nonlinear viscoelastic materials: Bioinspired applications and new characterization measures, Ph.D. thesis, Massachusetts Institute of Technology (2009).
- [14] Ewoldt RH, Winter P, Maxey J, McKinley GH: Large amplitude oscillatory shear of pseudoplastic and elastoviscoplastic materials, *Rheol. Acta* 49 (2010) 191–212.
- [15] Rogers SA: A sequence of physical processes determined and quantified in LAOS: An instantaneous local 2d/3d approach, *J. Rheol.* 56 (2012) 1129–1151.
- [16] Wilhelm M, Reinheimer P, Ortseifer M, Neidhöfer T, Spiess HW: The crossover between linear and non-linear mechanical behaviour in polymer solutions as detected by fourier-transform rheology, *Rheol. Acta* 39 (2000) 241–246.
- [17] Renou F, Stellbrink J, Petekidis G: Yielding processes in a colloidal glass of soft star-like micelles under large amplitude oscillatory shear (LAOS), *J. Rheol.* 54 (2010) 1219–1242.
- [18] Cho KS, Hyun K, Ahn KH, Lee SJ: A geometrical interpretation of large amplitude oscillatory shear response, *J. Rheol.* 49 (2005) 747–758.

- [19] Ewoldt RH, Hosoi AE, McKinley GH: New measures for characterizing nonlinear viscoelasticity in large amplitude oscillatory shear, *J. Rheol.* 52 (2008) 1427–1458.
- [20] Rogers SA, Erwin BM, Vlassopoulos D, Cloitre M: Oscillatory yielding of a colloidal star glass, *J. Rheol.* 55 (2011) 733–752.
- [21] Klein CO, Spiess HW, Calin A, Balan C, Wilhelm M: Separation of the nonlinear oscillatory response into a superposition of linear, strain hardening, strain softening, and wall slip response, *Macromolecules* 40 (2007) 4250–4259.
- [22] Rogers SA, Lettinga MP: A sequence of physical processes determined and quantified in large amplitude oscillatory shear (LAOS): Application to theoretical nonlinear models, *J. Rheol.* 56 (2012) 1–25.
- [23] Giacomini A, Bird R, Johnson L, Mix A: Large-amplitude oscillatory shear flow from the corotational Maxwell model, *J. Non-Newton Fluid Mech.* 166 (2011) 1081–1099.
- [24] Rogers SA, Erwin BM, Vlassopoulos D, Cloitre M: A sequence of physical processes determined and quantified in LAOS: Application to a yield stress fluid, *J. Rheol.* 55 (2011) 435–458.
- [25] Lauger J, Stettin H: Differences between stress and strain control in the non-linear behavior of complex fluids, *Rheol. Acta* 49 (2010) 909–930.
- [26] Celli JP, Turner BS, Afdhal NH, Ewoldt RH, McKinley GH, Bansil R, Erramilli S: Rheology of gastric mucin exhibits a pH-dependent sol–gel transition, *Biomacromolecules* 8 (2007) 1580–1586.
- [27] Nakano M, Yamamoto H: Dynamic viscoelasticity and its mechanical model of an mr suspension in oscillatory slit flow mode, *J. Intel. Mat. Syst. Str.* 10 (1999) 658–665.
- [28] Laun HM, Gabriel C, Kieburg C: Magnetorheological fluid (mrf) in oscillatory shear and parameterization with regard to mr device properties, *J. Phys. Conf. Ser.* 149 (2009) 012067.
- [29] Tiu C, Guo J, Uhlherr PHT: Yielding behaviour of viscoplastic materials, *J. Ind. Eng. Chem.* 12 (2006) 653–662.
- [30] Carrier V, Petekidis G: Nonlinear rheology of colloidal glasses of soft thermosensitive microgel particles, *J. Rheol.* 53 (2009) 245–273.
- [31] Le Grand A, Petekidis G: Effects of particle softness on the rheology and yielding of colloidal glasses, *Rheol. Acta* 47 (2008) 579–590.
- [32] Keentok M: The measurement of the yield stress of liquids, *Rheol. Acta* 21 (1982) 325–332.
- [33] Barnes HA, Walters K: The yield stress myth?, *Rheol. Acta* 24 (1985) 323–326.
- [34] Steffe JF: *Rheological methods in food process engineering*, Freeman Press, East Lansing (1996).
- [35] Boisly M, Kastner M, Brummund J, Ulbricht V: General aspects of yield stress fluids - terminology and definition of viscosity, *Appl. Rheol.* 24 (2014) 14578.
- [36] Gurnon AK, Wagner NJ: Large amplitude oscillatory shear (laos) measurements to obtain constitutive equation model parameters: Giesekus model of banding and nonbanding wormlike micelles, *J. Rheol.* 56 (2012) 333–351.
- [37] Pham KN, Petekidis G, Vlassopoulos D, Egelhaaf SU, Pusey PN, Poon WCK: Yielding of colloidal glasses, *Europhys. Lett.* 75 (2006) 624.
- [38] Pham KN, Petekidis G, Vlassopoulos D, Egelhaaf SU, Poon WCK, Pusey PN: Yielding behavior of repulsion- and attraction-dominated colloidal glasses, *J. Rheol.* 52 (2008) 649–676.
- [39] Koumakis N, Petekidis G: Two step yielding in attractive colloids: transition from gels to attractive glasses, *Soft Matter* 7 (2011) 2456–2470.
- [40] Laurati M, Egelhaaf SU, Petekidis G: Nonlinear rheology of colloidal gels with intermediate volume fraction, *J. Rheol.* 55 (2011) 673–706.
- [41] MacSporran WC, Spiers RP: The dynamic performance of the Weissenberg rheogoniometer. 3. Large-amplitude oscillatory shearing-harmonic analysis, *Rheol. Acta* 23 (1984) 90–97.
- [42] Mas R, Magnin A: Experimental validation of steady shear and dynamic viscosity relation for yield stress fluids, *Rheol. Acta* 36 (1997) 49–55.
- [43] Hilliou L, Wilhelm M, Yamanoi M, Goncalves MP: Structural and mechanical characterization of κ/ι -hybrid carrageenan gels in potassium salt using fourier transform rheology, *Food Hydrocolloid* 23 (2009) 2322–2330.
- [44] Dealy JM, Wissbrun KF: *Melt rheology and its role in plastics processing*, Van Nostrand Reinhold, New York (1990).
- [45] Brader JM, Siebenburger M, Ballauff M, Reinheimer K, Wilhelm M, Frey SJ, Weysser F, Fuchs M: Nonlinear response of dense colloidal suspensions under oscillatory shear: Mode-coupling theory and fourier transform rheology experiments, *Phys. Rev. E* 82 (2010) 061401.
- [46] Melito HS, Daubert CR, Foegeding EA: Creep and large amplitude oscillatory shear behavior of whey protein isolate/ κ -carrageenan gels, *Appl. Rheol.* 22 (2012) 63691.
- [47] Dimitriou CJ, Ewoldt RH, McKinley GH: Describing and prescribing the constitutive response of yield stress fluids using large amplitude oscillatory shear stress (laostress), *J. Rheol.* 57 (2013) 27–70.
- [48] Ewoldt RH: Defining nonlinear rheological material functions for oscillatory shear, *J. Rheol.* 57 (2013) 177–195.
- [49] Ng TSK, McKinley GH, Ewoldt RH: Large amplitude oscillatory shear flow of gluten dough: A model power-law gel, *J. Rheol.* 55 (2011) 627–654.
- [50] Ganeriwala SN, Rotz CA: Fourier transform mechanical analysis for determining the nonlinear viscoelastic properties of polymers, *Polym. Eng. Sci.* 27 (1987) 165–178.
- [51] Yu W, Wang P, Zhou C: General stress decomposition in nonlinear oscillatory shear flow, *J. Rheol.* 53 (2009) 215–238.
- [52] Lissajous MJ: Sur l’etude optique des mouvements vibratoires, *Ann. Chim. Phys.* 3 (1857) 147–242.
- [53] Philippoff W: Vibrational measurements with large amplitudes, *T. Soc. Rheol.* 10 (1966) 317–334.
- [54] Ewoldt RH, Hosoi AE, McKinley GH: An ontology for large amplitude oscillatory shear flow, *AIP Conf. Proc.* 1027 (2008) 1135–1137.
- [55] Haupt P: *Continuum mechanics and theory of materials*, Springer, Berlin, Heidelberg, New York (2002).
- [56] Hyun K, Baik ES, Ahn KH, Lee SJ, Sugimoto M, Koyama K: Fourier-transform rheology under medium amplitude oscillatory shear for linear and branched polymer melts, *J. Rheol.* 51 (2007) 1319–1342.
- [57] Hyun K, Ahn KH, Lee SJ, Sugimoto M, Koyama K: Degree of branching of polypropylene measured from fourier-transform rheology, *Rheol. Acta* 46 (2006) 123–129.

